OPEN ACCESS Freely available online

PLoS one

Computational Insights on the Competing Effects of Nitric Oxide in Regulating Apoptosis

Elife Z. Bagci[1,2], Yoram Vodovotz[3,4], Timothy R. Billiar[3], Bard Ermentrout[5]*, Ivet Bahar[1]*

1 Department of Computational Biology, McGowan Institute for Regenerative Medicine, University of Pittsburgh, Pittsburgh, Pennsylvania, United States of America, **2** Department of Biochemistry and Molecular Genetics, McGowan Institute for Regenerative Medicine, University of Pittsburgh, Pittsburgh, Pennsylvania, United States of America, **3** Department of Surgery, School of Medicine, McGowan Institute for Regenerative Medicine, University of Pittsburgh, Pittsburgh, Pennsylvania, United States of America, **4** Center for Inflammation and Regenerative Modeling, McGowan Institute for Regenerative Medicine, University of Pittsburgh, Pittsburgh, Pennsylvania, United States of America, **5** Department of Mathematics, Arts & Sciences, University of Pittsburgh, Pittsburgh, Pennsylvania, United States of America

Abstract

Despite the establishment of the important role of nitric oxide (NO) on apoptosis, a molecular- level understanding of the origin of its dichotomous pro- and anti-apoptotic effects has been elusive. We propose a new mathematical model for simulating the effects of nitric oxide (NO) on apoptosis. The new model integrates mitochondria-dependent apoptotic pathways with NO-related reactions, to gain insights into the regulatory effect of the reactive NO species N_2O_3, non-heme iron nitrosyl species (FeL_nNO), and peroxynitrite ($ONOO^-$). The biochemical pathways of apoptosis coupled with NO-related reactions are described by ordinary differential equations using mass-action kinetics. In the absence of NO, the model predicts either cell survival or apoptosis (a bistable behavior) with shifts in the onset time of apoptotic response depending on the strength of extracellular stimuli. Computations demonstrate that the relative concentrations of anti- and pro-apoptotic reactive NO species, and their interplay with glutathione, determine the net anti- or pro-apoptotic effects at long time points. Interestingly, transient effects on apoptosis are also observed in these simulations, the duration of which may reach up to hours, despite the eventual convergence to an anti-apoptotic state. Our computations point to the importance of precise timing of NO production and external stimulation in determining the eventual pro- or anti-apoptotic role of NO.

Citation: Bagci EZ, Vodovotz Y, Billiar TR, Ermentrout B, Bahar I (2008) Computational Insights on the Competing Effects of Nitric Oxide in Regulating Apoptosis. PLoS ONE 3(5): e2249. doi:10.1371/journal.pone.0002249

Editor: Kathrin Maedler, University of Bremen, Germany

Received November 14, 2007; **Accepted** March 2, 2008; **Published** May 28, 2008

Copyright: © 2008 Bagci et al. This is an open-access article distributed under the terms of the Creative Commons Attribution License, which permits unrestricted use, distribution, and reproduction in any medium, provided the original author and source are credited.

Funding: IB gratefully acknowledges the support from National Institutes of Health award No. 1P20-GM065805. GBE was supported by NSF DMS0513500.

Competing Interests: The authors have declared that no competing interests exist.

* E-mail: bahar@ccbb.pitt.edu (IB); bard@math.pitt.edu (BE)

Introduction

The survival of an organism depends on homeostatic mechanisms that establish a balance between cell proliferation and cell death. Apoptosis, a form of programmed cell death, assists in regulating cell proliferation. This process stands in contrast to necrosis, which is thought to be uncontrolled. Dysregulation of apoptosis has been implicated in various disease processes in which the cells apoptose to a higher or lower extent compared to those in healthy tissues [1]. When cells undergo apoptosis, a series of morphological and biochemical changes occur, the mechanisms of which are current topics of broad interest [2].

Apoptosis may be induced by various events, such as binding of extracellular (EC) death signaling ligands to host cell receptors, the lack of pro-survival signals, and genetic damage. These events are usually followed by the activation of caspases, **c**ysteine-dependent **asp**artate-specific prote**ase**s, which initiate and execute apoptosis. Caspases are activated through two major pathways: (a) ligand-dependent or receptor-induced activation (extrinsic pathway), involving death receptors such as Fas or the members of tumor necrosis factor (TNF) receptor superfamily, and (b) mitochondria-dependent activation (intrinsic pathway) via cytochrome *c* (cyt *c*) release from mitochondria, triggered by stress, irradiation or inflammation [3,4].

Binding of death ligands such as Fas ligand (FasL), TNF, or tumor necrosis-related apoptosis-inducing ligand (TRAIL) usually induces the oligomerization of associated receptors, followed by binding of adaptor proteins, e.g., Fas-Associated Death Domain proteins (FADD), to the cytoplasmic domains of the receptors [5]. The resulting Death Inducing Signaling Complex (DISC) recruits multiple procaspase-8 molecules that mutually cleave and activate one another into caspases-8 (casp8). In Type I cells, large quantities of casp8 activate other caspases including the executioner caspase-3 (casp3) molecules that ultimately lead to apoptosis. In Type II cells, on the other hand, the amount of casp8 activated at the DISC is small, such that the activation of casp8 does not propagate directly to casp3, but instead is amplified via the mitochondria.

Nitric oxide has opposite, competing effects in regulating apoptosis: it exerts an anti-apoptotic effect on hepatocytes [6–8], endothelial cells [9–13] and keratinocytes [14], whereas it is pro-apoptotic in the case of macrophages [15–18]. The variability and complexity of the effects of NO on ultimate cellular fate may arise from this molecule's ability to react with oxygen, reactive oxygen species, metal ions, small thiol-containing molecules, and proteins. The resulting reactive NO species can either trigger or suppress apoptosis through various mechanisms. Chief among them is the S-nitrosative suppression of caspase activation, subsequent to the generation of FeL_nNO or other species capable of carrying out S-nitrosation reactions (see below) [7,19]. Differences in the levels of NO and its reaction products may also arise from diverse inflammatory settings in which the expression of nitric oxide

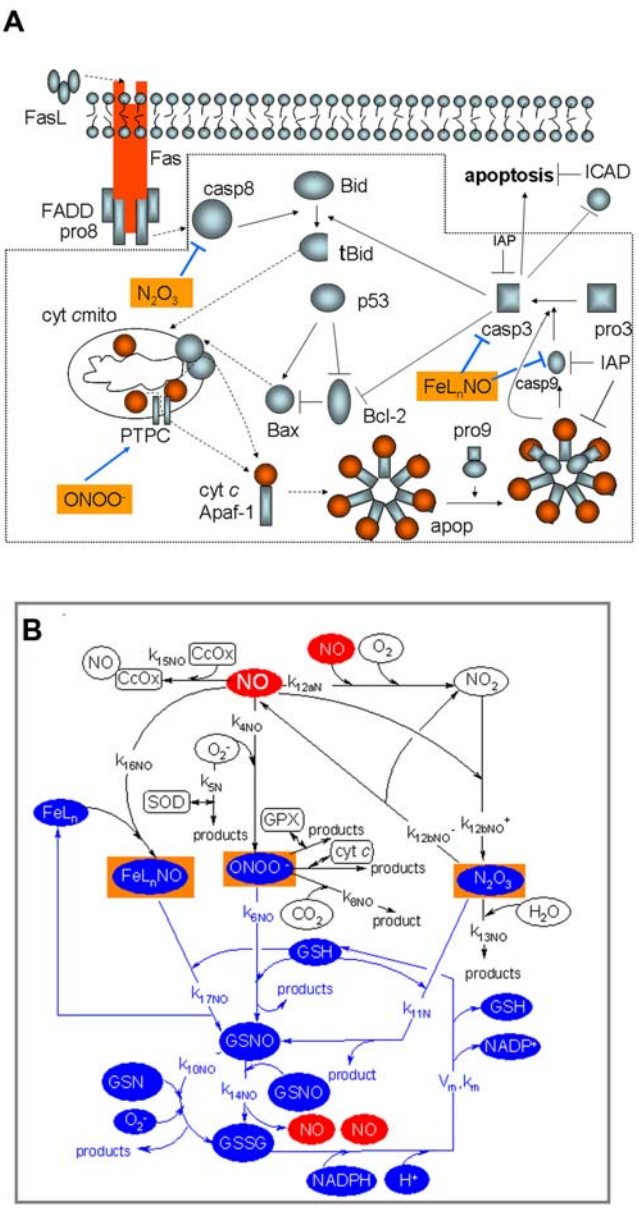

Figure 1. (A) Mitochondria-dependent apoptotic pathways in Model I. The dotted box includes the interactions considered in the model. Solid arrows indicate chemical reactions or upregulation; those terminated by a bar indicate inhibition or downregulation; and dashed arrows indicate subcellular translocation. The components of the model are procaspase-8 (pro8), procaspase-3 (pro3), procaspase-9 (pro9), caspase-8 (casp8), caspase-9 (casp9), caspase-3 (casp3), IAP (inhibitor of apoptosis), cytochrome *c* (cyt *c*), Apaf-1, the heptameric apoptosome complex (apop), the mitochondrial permeability transition pore complex (PTPC), p53, Bcl-2, Bax, Bid, truncated Bid (tBid). The reader is referred to our previous work [28] for more details. Three compounds (N_2O_3, FeL_nNO and $ONOO^-$) not included in the original Model I [28] are highlighted. These compounds establish the connection with the nitric oxide pathways delineated in panel B. (B) Nitric oxide (NO)-related reactions in Model II. The following compounds are included: $ONOO^-$ (peroxynitrite), GPX (glutathione peroxidase), O_2^- (superoxide), GSH (glutathione), GSNO (nitrosoglutathione), GSSG (glutathione disulfide), CcOX (cytochrome *c* oxidase), SOD (superoxide dismutase), FeL_n (non-heme iron compounds), FeL_nNO (non-heme iron nitrosyl compounds), NADPH (reduced form of nicotinamide adenine dinucleotide phosphate), NADP+ (oxidized form of nicotinamide adenine dinucleotide phosphate). FeL_nNO, $ONOO^-$ and N_2O_3, highlighted in both panels A and B, bridge between Models I to II. Model III integrates both sets of reactions/pathways through these compounds. GSH modulates their concentrations by reacting with them. GSH is converted by these reactions to GSNO, which is then converted to GSSG and finally back to GSH. Those compounds and interactions are shown in blue. See Table 1 for the complete list of reactions and rate constants.
doi:10.1371/journal.pone.0002249.g001

synthases (NOS) is affected. For example, quiescent endothelial cells express constitutive NOS (eNOS) that directly produce NO molecules and mediate so-called "direct" effects [20]. Some inflammatory stimuli, on the other hand, lead to inducible NOS (iNOS) expression that subsequently generates reactive NO species, which in turn mediate "indirect" effects of NO. The simultaneous presence of oxygen radicals can generate other reactive NO species that mediate further indirect effects of NO [20]. As another example, hepatocytes and macrophages have different amounts of non-heme iron complexes, which affect the levels of iron-nitrosyl species when NO is produced [21]. Finally, different intracellular levels of glutathione (GSH) can also modulate the time evolution of NO-related compounds [22].

Computational approaches have been used previously to help unravel the complex biology of NO. Biotransport of NO was first modeled by Lancaster [23,24] followed by other groups, among them Zhang and Edwards [25] (reviewed by Buerk [26]). Recently, Hu and coworkers focused on detailed reaction mechanism of NO [22]. These models have shed light into the biotransport of NO and the types of chemical reactions that involve NO and related reactive species. Additionally, a number of mathematical models have been proposed for understanding the mechanisms of apoptosis [27–35], including in particular the work of Eissing et al., which demonstrated the importance of IAP inhibition for imparting bistability in type I cells [30], and that of Rehm et al. [33] and Legewie et al. [32] that showed the same effect in type II cells. These studies have improved our understanding of the robustness of switch mechanisms for regulating apoptosis, but none of them has addressed the dichotomous effects of NO [27–35].

Herein, we propose a mathematical model that may shed light on the pro- and anti-apoptotic effects of NO in specific contexts. The model we propose couples the apoptotic cascade [28] to an extended model of NO reaction pathways initially proposed by Hu et al. [22]. First, we illustrate how identical cells can undergo apoptosis at different time points after being exposed to apoptotic stimuli, in accord with experimental data collected on single cells [36,37]. Then, we examine the apoptotic behavior in response to changes in N_2O_3, FeL_nNO, $ONOO^-$, and GSH levels in the presence of NO production by iNOS. Our simulations provide insights into the origin of the dichotomous effects of NO on apoptosis observed in experiments.

Results

First, we illustrate how different strengths of EC pro-apoptotic signals may result in opposite qualitative responses or different quantitative (time-dependent) responses in the same type of cells [37], using our recently introduced bistable model [28] (illustrated in Figure 1A). Then, we examine the differences in the bistable response of diverse NO producing cells, e.g. cells with different concentrations of GSH and FeL_n-and in different settings, i.e., with or without production of superoxide.

Delay in apoptosis induction (Model I)

Tyas et al. [37] showed that cells of the same type simultaneously subjected to EC stimuli initiate their apoptotic

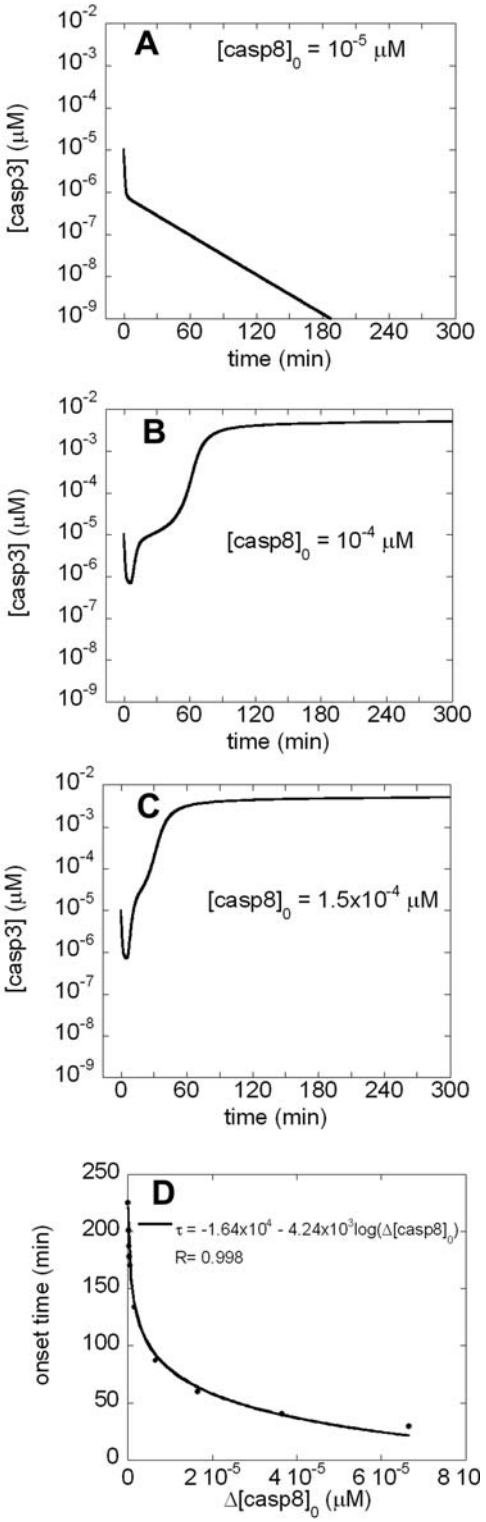

Figure 2. Time evolution of [casp3] predicted by a bistable model in response to different strengths of apoptotic stimuli, A) in a cell subjected to a weak EC apoptotic signal (reflected by the low concentration [caps8]$_0$); B) in a cell that is subjected to a stronger EC pro-apoptotic signal. Caspase-3 is activated at 60 minutes; C) in a cell that is subjected to a stronger EC pro-apoptotic signal than one in panel B. Caspase-3 is activated at 30 minutes. Panels A and B illustrate two opposite effects induced by different initial concentrations of caspase-8. The threshold concentration of [caps8]$_0$ required for the switch from anti-apoptotic to pro-apoptotic response is calculated to be 8.35×10^{-5} μM. Panels B and C illustrate the shift in the onset time of apoptosis depending on [casp8]$_0$. D) Dependence of apoptotic response time on the initial caspase-8 concentration. The ordinate is the onset time of caspase-3 activation, and the abscissa is the initial concentration of caspase-8 in excess of the threshold concentration required for the initiation of apoptosis (evidenced by increase in [casp3], see panels B–C). The onset time of caspase-3 activation exhibits a logarithmic decrease with Δ[casp8]$_0$ ([casp8]$_0$–8.35×10^{-5} μM).
doi:10.1371/journal.pone.0002249.g002

response at different times. Figure 2 panels A–C illustrate the theoretical time evolutions of casp3 in three identical cells subjected to different strengths of EC apoptotic stimuli (represented here by the initial concentration of casp8) in the absence of NO. For these simulations, we used Model I with three different values of [casp8]$_0$; 10^{-5} μM, 10^{-4} μM, and 1.5×10^{-4} μM in the respective panels A–C, while [casp3]$_0$ was 10^{-5} μM in all three cases. Panel A shows that low [casp8]$_0$ leads to the depletion of [casp3], while [casp8]$_0$ above a certain threshold (8.35×10^{-5} μM) (panels B and C) lead to increase in [casp3] and thereby onset of cell death. Furthermore, comparison of panels B and C shows that a relatively lower [casp8]$_0$ (or weaker EC apoptotic signal) results in a time-delayed initiation of apoptosis, in agreement with the single cell experiments done by Tyas et al. [37]. The sharp increase in [casp3] to its equilibrium level indeed starts about 30 minutes later in panel B, compared to panel C.

Next, we examined how this onset time varies with [casp8]$_0$. Figure 2D displays the results. An increase in onset time is predicted with decreasing [casp8]$_0$ up to [casp8]$_0 = 8.35\times10^{-5}$ μM, after which no apoptotic effect is observed. The time delay is found to obey a logarithmic decay with increasing Δ[casp8]$_0 \equiv$[casp8]$_0$–8.35×10^{-5} μM, as indicated by the best fitting curve.

This analysis shows that cells of the same type may undergo apoptosis at different times due to their different EC microenvironments. Hence, the difference in the onset times among cells of the same type in a given cell culture may be explained without recourse to alterations in the underlying network of biochemical reactions [28].

Nitric oxide-associated network (Model II) (Figure 1B)

The results from our calculations using Model II are shown in Figure 3. Here, we focused on the time evolution of four compounds, GSH, N_2O_3, FeL_nNO and $ONOO^-$, displayed in respective panels A–D. The NO species N_2O_3, FeL_nNO and $ONOO^-$ have been proposed to carry out various indirect effects of NO on cellular pathways, including apoptosis, during inflammation [20].

GSH is an anti-oxidant reduced to GSSG by reacting with nitrosative N_2O_3 and FeL_nNO, and with oxidative $ONOO^-$ (Table 1). GSH is depleted to low levels in a switch-like manner due to those reactions (panel A). The depletion of GSH is accompanied by increases in N_2O_3 and FeL_nNO concentrations (panels B–C). On the other hand, this switch-like behavior is not that pronounced in [$ONOO^-$] time dependence (panel D). Simulations performed with different initial GSH concentrations (three different curves in each panel) change the steady-state concentrations of all three NO-related compounds that interfere with apoptotic pathways (panels B–D). The switch-like increase in [N_2O_3] and non-switch-like increase in [$ONOO^-$] is in agreement with the results of Hu et al. [22].

Anti-apoptotic and pro-apoptotic effects of NO (Model III)

We analyze here the dynamics of the reduced mitochondria-dependent apoptosis model coupled to anti- and pro-apoptotic

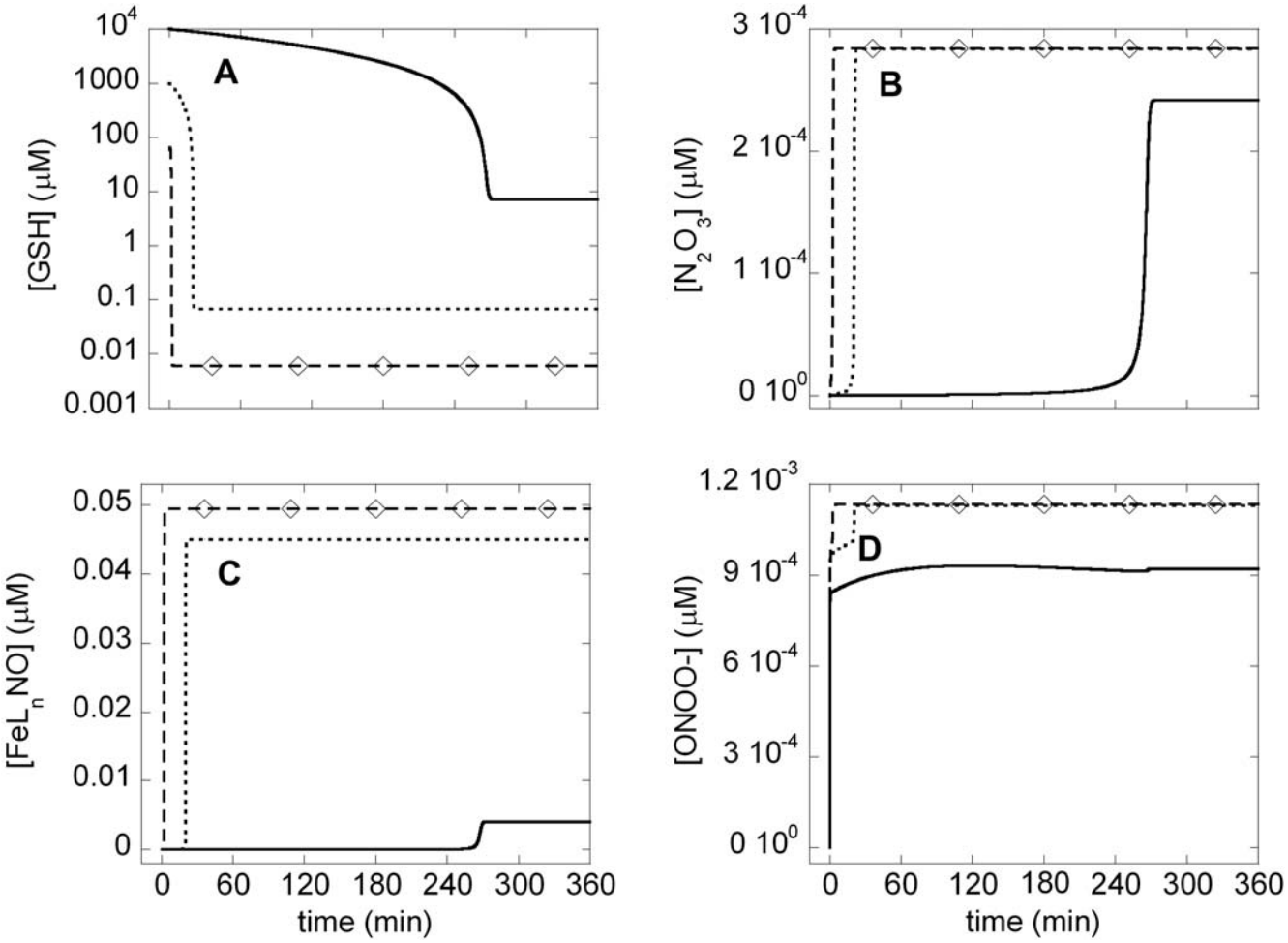

Figure 3. Time evolutions of A) GSH, B) N_2O_3, C) FeL_nNO, and D) $ONOO^-$ predicted by Model II. N_2O_3 and FeL_nNO increase to high concentrations by a switch-like mechanism induced by a decrease in GSH concentration due to conversion of GSH to GSNO and subsequently to GSSG. $[ONOO^-]$ does not follow a similar switch-like increase in its concentration. Solid curve is for $[GSH]_0 = 10^4$ μM, dotted curve for $[GSH]_0 = 10^3$ μM, and dashed curve with diamonds for $[GSH]_0 = 10^2$ μM. The response is thus sharper and earlier in the presence of lower initial concentrations of GSH.
doi:10.1371/journal.pone.0002249.g003

pathways associated with NO; see Materials and Methods for the list of reactions/interactions/steps that come into play in this model (III). As mentioned above, NO-related pathways are coupled to apoptotic pathways through N_2O_3, FeL_nNO, and $ONOO^-$ that are produced by the reaction of NO with O_2, FeL_n and O_2^-, respectively. For simplicity, those effects of NO mediated by cGMP [38,39] are not included in this initial mathematical model.

Modulating roles of N_2O_3 and GSH in apoptosis. We initially excluded non-heme iron compounds in order to assess the effect of N_2O_3 exclusively. The production rate of superoxide was likewise assumed to be zero. N_2O_3 is produced by reactions *(xii)* and *(xiii)* in Table 1. NO production and EC stimulation were initiated simultaneously. Figures 4A–C are the counterparts of Figures 2A–C, respectively (same initial conditions, except for the interference of NO pathways through N_2O_3), where the time-dependence of [casp3] (solid curve) and [GSH] are shown. The bistable response to apoptotic stimuli, dependent on $[casp8]_0$, is shown to be maintained despite the interference of NO pathways through N_2O_3. The three columns refer to different initial concentrations of GSH, decreasing from $[GSH]_0 = 10^3$ (Panels A–C), to $[GSH]_0 = 10^2$ (panels D–F) and $GSH]_0 = 0$ (panels G–I). The threshold $[casp8]_0$ value for casp3 activation was 8.35×10^{-5} μM in Figure 2, where NO was not produced at all. This value remains the same for both $[GSH]_0 = 10^4$ μM (not shown) and 10^3 μM (panels A–C) in the presence of NO, but increases to 9.9×10^{-5} μM when $[GSH]_0$ is 10^2 μM (panels D–F) and to 1.26×10^{-4} μM when $[GSH]_0$ is zero (panels G–I), hence the different (pro-apoptotic) behavior observed in panel H.

These results suggest that N_2O_3 does not affect the bistable character of the response to EC stimuli, except for modifying the threshold for onset of apoptosis, which is shifted to higher $[casp8]_0$ (i.e. rendered more difficult) with decreasing $[GSH]_0$. However, high initial concentrations of GSH restore the threshold back to 8.35×10^{-5} μM. Therefore, N_2O_3 can serve as an effective modulator of apoptosis provided that the level of GSH in the system is sufficiently low.

Effect of N_2O_3 on the threshold degradation rates of Bax for transition from bistable to monostable behavior. In our previous computational study of apoptotic pathways, we observed a bistable behavior (selecting between cell death and survival) for degradation rates of Bax (μ_{Bax}) lower than a threshold value ($0.11\ s^{-1}$), while monostable cell survival was predicted when $\mu_{Bax} > 0.11\ s^{-1}$ (Figure 4A in Ref. [28]). This critical value of

Table 1. Reactions in Model II

Description of the reaction/interaction	Rate constant (*)	Reference	Reaction index
Production of NO	$k_{1NO} = 1\ \mu M/s$	[22]	(i)
Production of O_2^-	$k_{2NO} = 0.1\ \mu M/s$	[22]	(ii)
Production of GSH	$k_{3NO} = 0$	[22]	(iii)
$NO+O_2^- \rightarrow ONOO^-$	$k_{4NO} = 6700\ \mu M^{-1}s^{-1}$	[56]	(iv)
$SOD+O_2^-+H^+ \rightarrow SOD+½\ O_2+½\ H_2O_2$	$k_{5NO} = 2400\ \mu M^{-1}s^{-1}$	[57]	(v)
$ONOO^-+GSH \rightarrow GSNO+products$	$k_{6NO} = 0.00135\ \mu M^{-1}s^{-1}$	[58]	(vi)
$ONOO^-+GPX \rightarrow GPX+products$	$k_{7NO} = 2\ \mu M^{-1}s^{-1}$	[59]	(vii)
$ONOO^-+CO_2 \rightarrow products$	$k_{8NO} = 0.058\ \mu M^{-1}s^{-1}$	[60,61]	(viii)
$ONOO^-+cyt\ c \rightarrow cyt\ c+products$	$k_{9NO} = 0.025\ \mu M^{-1}s^{-1}$	[62]	(ix)
$2GSNO+O_2^-+H_2O \rightarrow GSSG+products$	$k_{10NO} = 0.0006\ \mu M^{-2}s^{-1}$	[63]	(x)
$N_2O_3+GSH \rightarrow GSNO+NO_2^-+H^+$	$k_{11NO} = 66\ \mu M^{-1}s^{-1}$	[64]	(xi)
$2NO+O_2 \rightarrow 2NO_2$	$k_{12aNO} = 0.000006\ \mu M^{-2}s^{-1}$	[65]	(xii)
$NO_2+NO \leftrightarrow N_2O_3$	$k_{12bNO}^+ = 1100\ \mu M^{-1}s^{-1}$	[65]	(xiii)
	$k_{12bNO}^- = 81000\ s^{-1}$		
$N_2O_3+H_2O \rightarrow products$	$k_{13NO} = 1600\ s^{-1}$	[65,66]	(xiv)
$GSSG+NADPH+H^+ \rightarrow 2GSH+NADP^+$	$V_m = 320\ \mu Ms^{-1}$	[67]	(xv)
	$K_m = 50\ \mu M$		
$Cu^+\ GSNO \rightarrow ½\ GSSG+NO$	$k_{14NO} = 0.0002\ s^{-1}$	[68,69]	(xvi)
$CcOx+NO \rightarrow CcOX.NO$	$k_{15NO} = 100\ \mu M^{-1}s^{-1}$	[70]	(xvii)
$FeL_n+NO \rightarrow FeL_nNO$	$k_{16NO} = 1.21\ \mu M^{-1}s^{-1}$	[71]	(xviii)
$FeL_nNO+GSH \rightarrow GSNO+FeL_n$	$k_{17NO} = 66\ \mu M^{-1}s^{-1}$ [a]	[72]	(xix)
$GSH+O_2^- \rightarrow ½\ GSSG+products$	$k_{17bNO} = 0.0002\ \mu M^{-1}s^{-1}$	[73]	(xx)

[a]Same as k_{11NO}

doi:10.1371/journal.pone.0002249.t001

μ_{Bax} for the transition from bistability to monostability is called a limit point. We explored how the inclusion of NO reactions affects these findings. The limit point value of the Bax degradation rate for monostable cell survival is found to remain unchanged (at $0.11\ s^{-1}$) for the range $10^3 \leq [GSH]_0 \leq 10^4\ \mu M$. However, it decreases to $0.098\ s^{-1}$ for $[GSH]_0 = 10^2\ \mu M$ and $0.096\ s^{-1}$ for $[GSH]_0 = 0\ \mu M$ in the present model. The model again predicts that N_2O_3 is not influential when the GSH level is sufficiently high in the cell.

Roles of non-heme iron complexes and GSH in apoptotic response. One of the important anti-apoptotic effects of NO is presumed to occur via its ability to react with non-heme iron complexes (FeL_n) to form FeL_nNO. These species inhibit caspases by S-nitrosating the catalytic cysteine in the active site of these enzymes [19,40,41].

The results are presented in Figure 5, panels A-F, organized similarly to Figure 4 (i.e. using different $[casp8]_0$ in each row, and different $[GSH]_0$ in the two columns). Our calculations suggest that when the FeL_n concentration is higher than 0.03 μM, there are no longer two stable steady-states at long times: caspase-3 levels always decrease to zero, even though their time evolutions depend on $[casp8]_0$ and $[GSH]_0$. Yet, depending on the level of GSH, both apoptosis and cell survival may be possible. Panels A–C correspond to relatively high $[GSH]_0$. In panel A, [casp3] decreases to 10^{-8} μM that is less than 1 molecule per cell, hence zero, from 10^{-5} μM within the first two hours. However, in panels B and C, [casp3] increases to nanomolar values and remains at those levels for more than three hours. Caspase-3 may cause enough damage to kill the cell before it is depleted at longer times. We note that lower $[GSH]_0$ (e.g. $[GSH]_0 = 10^3$ μM, panels D–F and $[GSH]_0 < 10^3$ μM, data not shown) do not permit the casp3 concentration to reach such pro-apoptotic levels and monostable cell survival is observed irrespective of $[casp8]_0$.

Various cell types subject to different intracellular microenvironments, or even the same cells under different settings (e.g. healthy state vs. inflammation or oxidative stress), may produce or experience different reactive NO intermediates [7,20,42]. For example, more FeL_nNO may be produced in hepatocytes than in RAW264.7 macrophage-like cells due to the high level of non-heme iron complexes in hepatocytes [21]. In our previous study, RAW264.7 cells underwent apoptosis in the presence of NO; conversely, no casp3 activation was observed in either hepatocytes or iron loaded RAW264.7 cells [21]. The results (Figure 4 and data not shown) suggest that in cells with iron concentrations lower than 0.03 μM (e.g. RAW264.7 cells), both cell survival and apoptosis are possible depending on the strength of apoptotic stimuli (in agreement with our experimental results) [21]. However, a change in the intracellular environment of the same cell can change the response. Figure 5D–F shows that casp3 is not activated in the presence of non-heme iron ($[FeL_n]_0 = 0.05\ \mu M$) when $[GSH]_0 = 10^3$ μM and $[GSH]_0 < 10^3$ μM (data not shown). We also checked if casp3 is activated when $[casp8]_0$ is as high as 0.1 μM when $[GSH] = 10^3$ μM. In this case, caspase-3 concentration increased to 0.0007 μM for approximately 5 minutes, an apoptotic stimulus that is likely insufficient for apoptosis. This prediction is in good agreement with our observation that caspase-3 is not activated in non-heme iron-loaded RAW264.7 cells whose $[GSH]_0$ does not reach 10^4 μM [21].

Roles of $ONOO^-$ and GSH in apoptotic response. The mechanism by which NO or its reactive species exert pro-

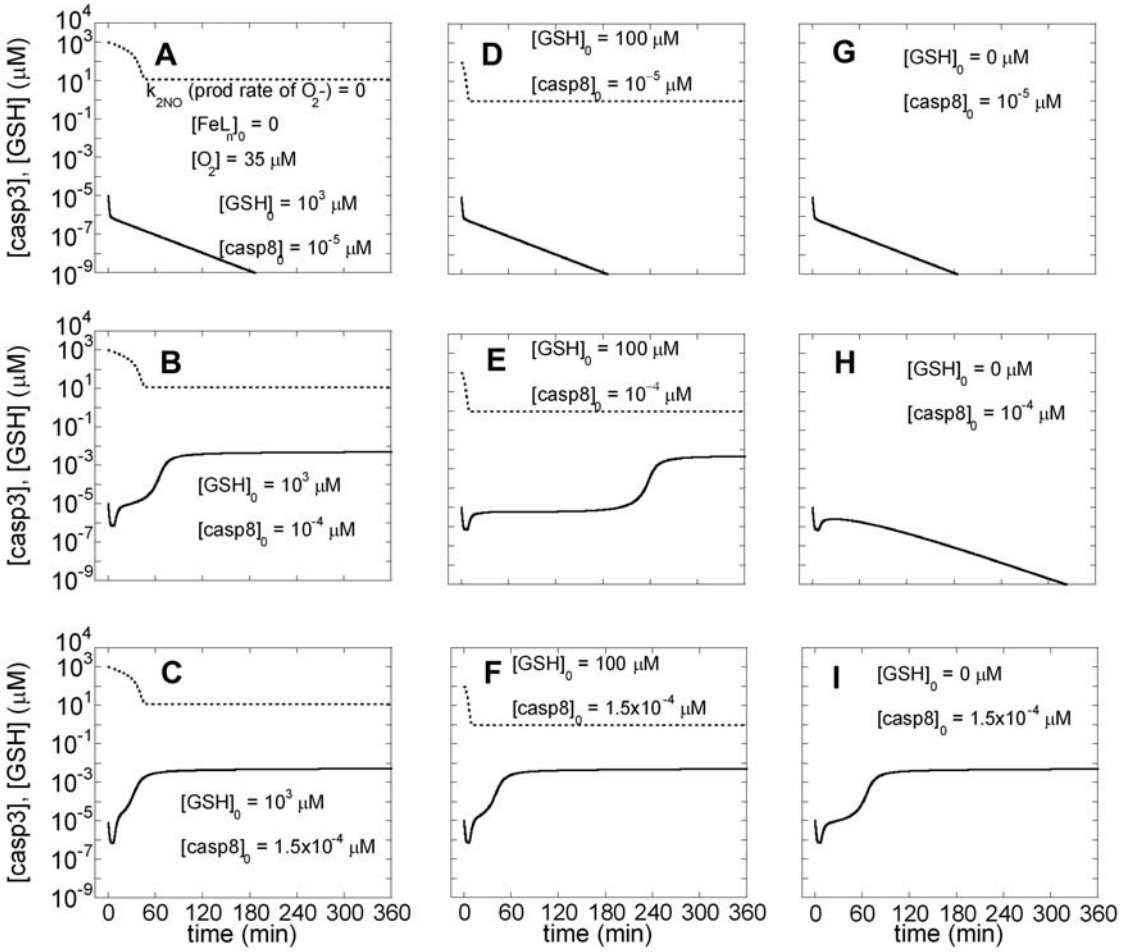

Figure 4. Time evolutions of [GSH] and [casp3] predicted by Model III in the presence of N_2O_3 effects. Here, in order to visualize the effect of N_2O_3 exclusively, the reaction *(xxii)* in Table 4 is included in the model while those involving FeL_nNO and $ONOO^-$ (reactions (*xx, xxiii-xxv*) are not, assuming FeL_n concentration and rate of formation of superoxide to be zero. The solid curves depict the time evolution of [casp3], and dotted curves refer to [GSH]. The three rows of panels are the counterparts of those in Figure 2 A–C, with the different columns referring to different initial concentrations of GSH: A–C) $[GSH]_0 = 10^3$ μM; D–F) $[GSH]_0 = 10^2$ μM; G–I) $[GSH]_0 = 0$ μM.
doi:10.1371/journal.pone.0002249.g004

apoptotic effects is not well established [43]. In the present study, we assume that the pro-apoptotic effect of NO occurs via formation of $ONOO^-$, as has been suggested from a large number of experimental studies both *in vitro* and *in vivo* [44,45]. Experimental studies suggest that $ONOO^-$ may induce the opening of mitochondrial permeability transition pores (MPTPs) and subsequent cyt *c* release from mitochondria [38].

The possible mechanisms of cyt *c* release from mitochondria are diverse and controversial [46,47]. In our model, we assume that cyt *c* release is mediated by activation of MPTPs, independent of Bax channel formation on mitochondria. The complex that forms the MPTPs is called mitochondrial permeability transition pore complex (PTPC). The complex consists of peripheral benzodiazepine receptor, cyclophilin D, adenine nucleotide translocator (ANT), voltage-dependent anion channel (VDAC), and other proteins [48]. ANT is proposed to be converted from a specific transporter to a non-specific pore which then releases cyt *c* into the cytoplasm and subsequently induces apoptosis. It has been suggested that $ONOO^-$ acts on PTPC, specifically on ANT, to convert it to a non-specific pore ($PTPC_{act}$) [49]. We represent this process as:

$$ONOO^- + \text{PTPC} \rightarrow \text{PTPC}_{act} + \text{products}$$

Cytochrome *c* is then released from the pore formed by $PTPC_{act}$

$$\text{cyt } c_{mito} + \text{PTPC}_{act} \rightarrow \text{cyt } c + \text{PTPC}_{act}$$

The results are shown in Figure 6. The initial concentration of PTPC is assumed to be high (0.01 μM). At that value, Model I predicts the response to apoptotic stimuli to be monostable apoptosis (Figure 6 in Ref. [28]). We see a similar response in Figure 6A; a low initial value of casp8 (10^{-5} μM) results in an increase of [casp3] to nanomolar levels. Casp3 activation was observed with even lower values of $[casp8]_0$. However, casp3 does not reach nanomolar concentrations when $[GSH]_0 = 10^3$ μM (Figures 6D–F) and $[GSH]_0 < 10^3$ μM (data not shown). Initial concentrations $[casp8]_0$ higher than 1.5×10^{-4} μM did not change this prediction.

These results suggest that in cells with large numbers of MPTPs (probably with high numbers of mitochondria), there are two possible outcomes in the presence of NO and O_2^- production:

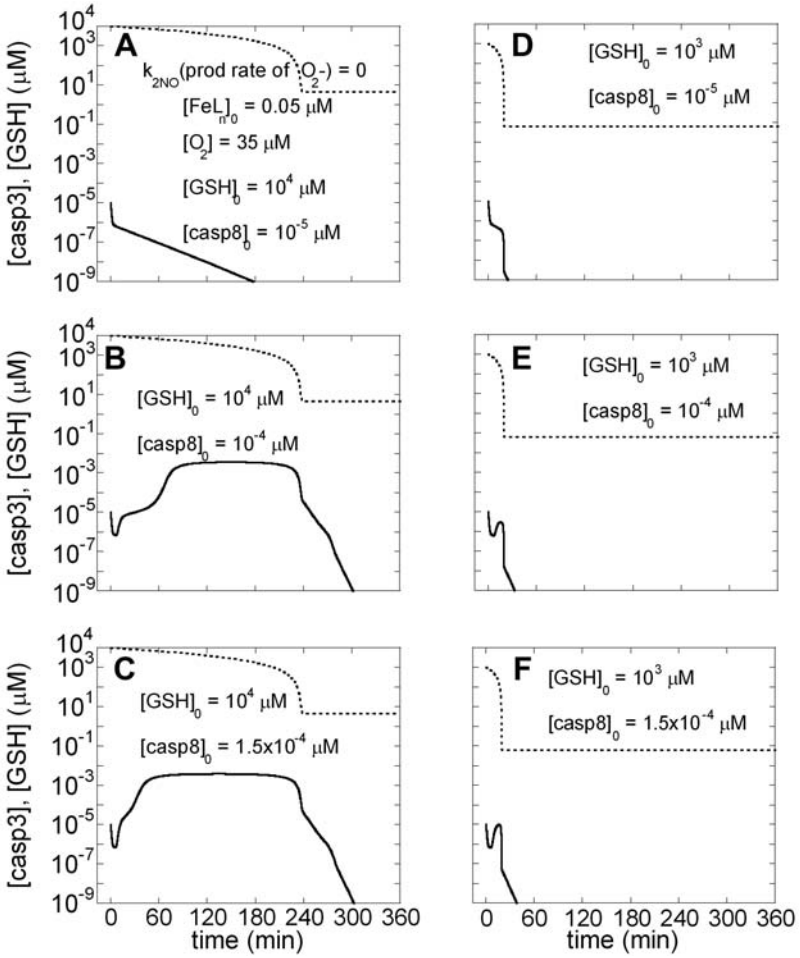

Figure 5. Time evolutions of [GSH] and [casp3] predicted by Model III in the presence of N_2O_3 and FeL_nNO. N_2O_3 is present in the model ($[O_2]$ is non-zero) as well as FeL_nNO ($[FeL_n]_0$ is non-zero). Each column is a counterpart of Figure 2A–C with different initial concentrations of GSH. A–C) $[GSH]_0 = 10^4$ μM; D–F) $[GSH]_0 = 10^3$ μM. Solid curve shows the time evolution of [casp3] and dotted curve that of [GSH].
doi:10.1371/journal.pone.0002249.g005

pathological cell death when GSH level is high (10^4 μM) and solely cell survival when GSH level is low ($[GSH] \leq 10^3$ μM) in the presence of O_2 and FeL_n. This result stands in contrast with studies in which GSH protects against oxidative stress (high concentrations of O_2^- and $ONOO^-$) that can cause apoptosis. The reason for this paradoxical prediction is that GSH has both protective and pro-apoptotic effects in our simulations: it exerts apoptotic effects via its reaction with anti-apoptotic N_2O_3 and FeL_n, and protective effects due to its reaction with pro-apoptotic O_2^- and $ONOO^-$. Simulations (Figure 6) suggest that the pro-apoptotic effect of GSH is stronger than its protective effect using the interactions and parameters adopted in current simulations.

To examine the possibility of an alternative response, we repeated the computations depicted in Figure 6 in the absence of O_2 (so that N_2O_3 is not produced) and FeL_n. We also used initial PTPC concentration of 0.0001 μM, at which Model I predicts bistability (Figure 6 in ref [28]). As seen in Figure 7, both cell survival and apoptosis are possible under these conditions, depending on $[casp8]_0$. Higher $[GSH]_0$ (10^4 μM) results in cell survival (Figure 7B) in contrast to lower $[GSH]_0$ resulting in apoptosis (Figure 7E) under the same amount of EC stimulus ($[casp8]_0 = 7 \times 10^{-5}$ μM). The present analysis thus shows that the protection by GSH against oxidative stress is possible provided that O_2 and FeL_n levels are sufficiently low.

Discussion

We present here the results from simulations that incorporate the main chemical interactions of NO with components of the apoptotic interactions network, with the goal of shedding light on the dichotomous effects of NO on apoptosis. Based on previously published studies, we considered N_2O_3 and FeL_nNO to be anti-apoptotic and $ONOO^-$ pro-apoptotic. The results predict that cell survival or apoptosis is determined by a complex interplay among these reactive NO species and GSH. We observed that relative concentrations of anti-apoptotic and pro-apoptotic species determine the ultimate cell fate at late time points. Interestingly, transient apoptotic effects were observed under specific conditions (e.g. Figure 5 panels B–C). These intriguing findings point to the importance of the *timing* of NO production and apoptotic stimuli in determining the actual anti- or pro-apoptotic effect, even if steady state conditions favor cell survival, in agreement with our previous observations [50–52]. Another interesting effect we observed in our simulations was the time shift/delay in the onset of apoptosis in the presence of weak EC stimulus (panel B–D in Figure 2), consistent with the experiments of Tyas et al. [37].

Our simulations suggest that N_2O_3 and non-heme iron nitrosyl form in a switch-like manner after depletion of GSH. $ONOO^-$ formation, on the other hand, hardly shows any switch-like

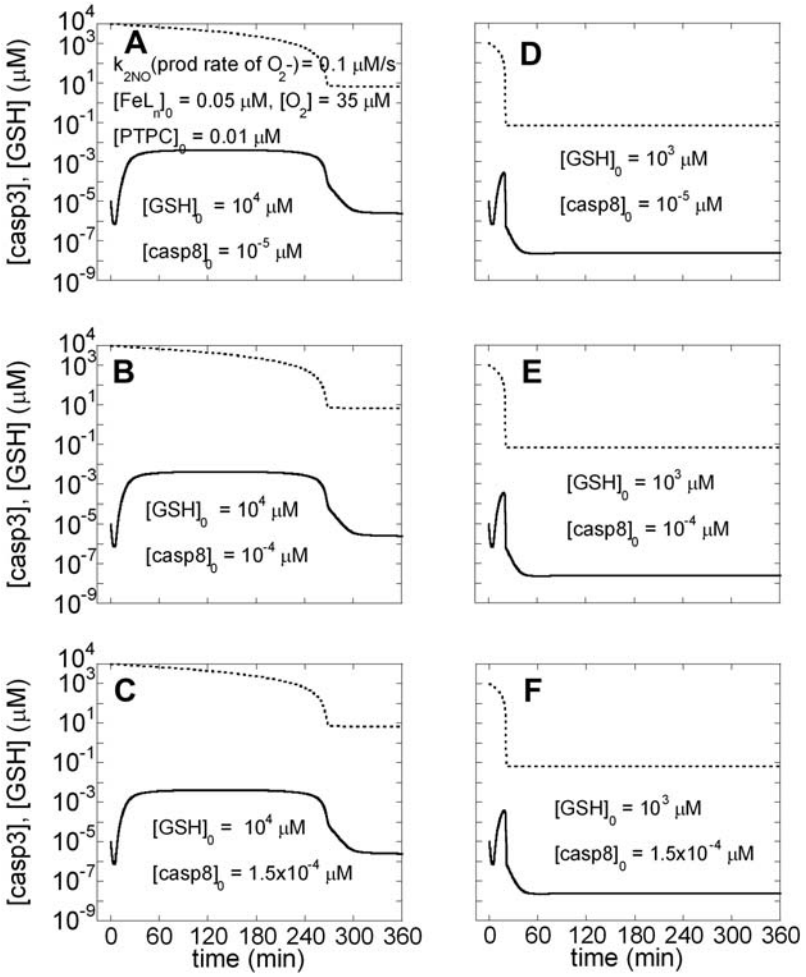

Figure 6. Time evolutions of [GSH] and [casp3] predicted by Model III in the presence of N_2O_3, FeL_nNO and $ONOO^-$. The initial concentration of PTPC is 0.01 μM. Each column is a counterpart of Figure 2A–C and has a different initial concentration for GSH. A–C) $[GSH]_0 = 10^4$ μM; D–F) $[GSH]_0 = 10^3$ μM. Solid line is for time evolution of [casp3] and dashed line is for time evolution of [GSH]. Caspase-3 concentrations at long times are 2.4 $\times 10^{-4}$ μM and 2.5$\times 10^{-8}$ μM for panels A–C and D–F, respectively.
doi:10.1371/journal.pone.0002249.g006

behavior. We further found that N_2O_3 does not eliminate the bistability between cell survival and apoptosis, but rather increases the threshold $[casp8]_0$ for onset of apoptosis. However, high initial concentrations of GSH restore the threshold back to its original value. Therefore, we would predict, non-intuitively, that N_2O_3 does not influence cell survival when $[GSH]_0$ level is high.

On the other hand, our simulations suggest that there are no longer two stable steady states (cell survival and apoptosis) in the presence of non-heme iron at a level higher than a threshold value. Caspase-3 levels always decrease to zero even though its time evolution may depend on $[casp8]_0$ and $[GSH]_0$. Yet, despite the steady state conditions that favor cell survival, executioner caspase concentrations can reach and retain apoptotic levels for several hours before they level off, when $[GSH]_0$ is high. When $[GSH]_0$ is low, on the other hand, our simulations predict resistance to apoptosis, in agreement with experimental observation [21].

In cells with high numbers of MPTPs (probably cells that contain high numbers of mitochondria), our simulations suggest two possibilities in the presence of simultaneous NO and O_2^- production and sufficiently high $[FeL_n]_0$: pathological cell death when $[GSH]_0$ is high (10^4 μM) or solely cell survival when $[GSH]_0$ level is low ($[GSH]_0 \leq 10^3$ μM). On the other hand, GSH is protective against oxidative stress when O_2 and FeL_n levels are low in cells with low numbers of MPTPs.

Tiedge et al. [53] have shown that pancreatic beta cells have low anti-oxidant levels (notably, GSH) and that the number of mitochondria is a determining factor in survival. They have also shown that transfection of the cells with a peroxide-inactivating enzyme, catalase, can protect against high-glucose induced apoptosis. An interesting experiment would be to correlate the number of mitochondria in the transfected cells with their survival. Oyadomari et al. [54] have shown that the endoplasmic reticulum (ER) plays a crucial role in the fate of NO-sensitive beta cells via calcium signaling. A natural next step in the present model would be to include these effects via a model which incorporates the effects of NO on the ER.

Our results are subject to several limitations. While we have adopted values for kinetic parameters and concentrations in accord with experimental data whenever available (Tables 1 and 2), many of the true intracellular rate constants for the reactions in our simulations are unknown. Given that the observed apoptotic responses are so sensitive to model parameters, detailed knowledge of reaction mechanisms and accurate values of rate constants are needed in modeling reaction networks as complicated as the ones

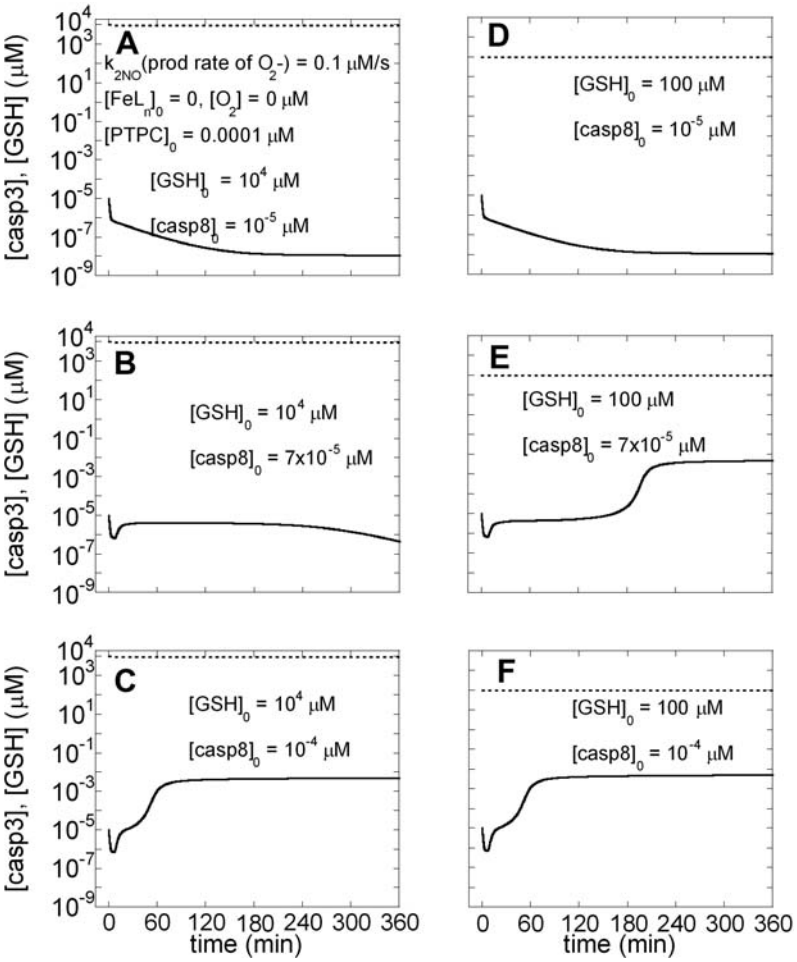

Figure 7. Time evolutions of [GSH] and [casp3] predicted by Model III in the absence of N_2O_3, FeL_nNO and presence of $ONOO^-$. The initial concentration of PTPC is 0.0001 μM. A–C) $[GSH]_0 = 10^4$ μM; D–F) $[GSH]_0 = 10^2$ μM. Solid line is for time evolution of [casp3] and dashed line is for time evolution of [GSH].
doi:10.1371/journal.pone.0002249.g007

presented here. Due to an extensive literature basis, we have posited that the pro-apoptotic NO species is $ONOO^-$; however, other species may in fact exert this effect. Additionally, the hypotheses raised by our simulations remain to be tested by further experiments. Some of the predictions could be tested by iron chelation and/or treatment with superoxide donors in a cell-free system or in single-cell studies, though each of these manipulations may have additional, artifactual effects. The hypothesis of bistability with regards to the apoptotic response can be tested as suggested by Legewie et al. [32], either in cell free-systems by adding caspase-3 or in single living cells by microinjecting caspase-3. The time evolution of caspase-3 can be monitored by fluorescent caspase-3 substrates. The time needed for caspase-3 activation will increase abruptly as caspase-3 concentration added will approach threshold value in a bistable system (Figure 2D). Such combined experimental and computational studies may potentially help us understand and design therapeutics for diseases associated with apoptosis dysregulation.

Materials and Methods

Models

Three models are considered in this study. **Model I**, proposed in our earlier work [28], focuses on the pathways involved in mitochondria-dependent apoptosis (Figure 1A). **Model II** is an extension of the kinetic model of NO-associated reactions recently proposed by Hu et al. [22] (Figure 1B). Finally, **Model III** is the integration of Models I and II, proposed in the present study, to examine the pro-apoptotic and anti-apoptotic effects of NO.

Table 2. Equilibrium levels and initial concentrations used in Model II

Equilibrium concentrations	**References**
$[SOD]_\infty = 10$ μM	[74]
$[GPX]_\infty = 5.8$ μM	[67]
$[CO_2]_\infty = 10^3$ μM	[61]
$[O_2]_\infty = 35$ μM	[67]
$[cyt\ c]_\infty = 400$ μM	[75]
Initial concentrations	**References**
$[CcOx]_0 = 0.1$ μM	[76]
$[FeL_n]_0 = 0.05$ μM	[77]
$[GSH]_0 = 10^4$ μM (or otherwise specified)	[22]

doi:10.1371/journal.pone.0002249.t002

Table 3. Rate equations for Model II (*)

Rate laws (Eq.s 1–20) and differential rate equations (Eq.s 21–29)	Equation numbers
$r_{1NO} = k_{1NO}$	(1)
$r_{2NO} = k_{2NO}$	(2)
$r_{3NO} = k_{3NO}$	(3)
$r_{4NO} = k_{4NO}[NO][O_2^-]$	(4)
$r_{5NO} = k_{5NO}[SOD][O_2^-]$	(5)
$r_{6NO} = k_{6NO}[ONOO^-][GSH]$	(6)
$r_{7NO} = k_{7NO}[ONOO^-][GPX]$	(7)
$r_{8NO} = k_{8NO}[ONOO^-][CO_2]$	(8)
$r_{9NO} = k_{9NO}[ONOO^-][cyt\ c]$	(9)
$r_{10NO} = k_{10NO}[GSNO]^2[O_2^-]$	(10)
$r_{11NO} = k_{11NO}[N_2O_3][GSH]$	(11)
$r_{12aNO} = k_{12aNO}[NO]^2[O_2]$	(12)
$r_{12bNO}^+ = k_{12bNO}^+[NO_2][NO]$	(13)
$r_{12bNO}^- = k_{12bNO}^-[N_2O_3]$	(14)
$r_{13NO} = k_{13NO}[N_2O_3]$	(15)
$r_m = V_m[GSSG]/(K_m+[GSSG])$	(16)
$r_{14NO} = k_{14NO}[GSNO]$	(17)
$r_{15NO} = k_{15NO}[CcOx][NO]$	(18)
$r_{16NO} = k_{16NO}[FeL_n][NO]$	(19)
$r_{17NO} = k_{17NO}[FeL_nNO][GSH]$	(20)
$d[NO]/dt = r_{1NO}-r_{4NO}-2r_{12aNO}-r_{12bNO}^+ + r_{12bNO}^- + r_{14NO} - r_{15NO} - r_{16NO}$	(21)
$d[O_2^-]/dt = r_{2NO}-r_{4NO}-r_{5NO}-r_{10NO}$	(22)
$d[ONOO^-]/dt = r_{4NO}-r_{6NO}-r_{7NO}-r_{8NO}-r_{9NO}$	(23)
$d[GSH]/dt = r_{3NO}-r_{6NO}-r_{11NO}+2r_m-r_{17NO}$	(24)
$d[GSNO]/dt = r_{6NO}-2r_{10NO}+r_{11NO} - r_{14NO}+r_{17NO}$	(25)
$d[N_2O_3]/dt = -r_{11NO}+r_{12bNO}^+ - r_{12bNO}^- - r_{13NO}$	(26)
$d[NO_2]/dt = 2r_{12aNO}-r_{12bNO}^+ + r_{12bNO}^-$	(27)
$d[CcOx]/dt = -r_{15NO}$	(28)
$d[FeL_n]/dt = -r_{16NO}+r_{17NO}$	(29)

(*) Note that $[FeL_nNO] = [FeL_n]_0 - [FeL_n]$, and $[GSSG] = ([GSH]_0 - [GSH] - [GSNO])/2$
doi:10.1371/journal.pone.0002249.t003

All interactions (chemical or physical; single step or multiple steps) are modeled using mass action kinetics theory and methods. The simulations are performed using XPPAUT software (http://www.math.pitt.edu/~bard/xpp/xpp.html) [55].

Table 5. The modified equations from either Model I or II (*)

Rate laws (Eq.s 30–34) and differential rate equations (Eq.s 35–43)	Equation numbers
$r_{18NO} = k_{18NO}[ONOO^-][PTPC]$	(30)
$r_{19NO} = k_{19NO}[N_2O_3][casp8]$	(31)
$r_{20NO} = k_{20NO}[FeL_nNO][casp8]$	(32)
$r_{21NO} = k_{21NO}[FeL_nNO][casp9]$	(33)
$r_{22NO} = k_{22NO}[FeL_nNO][casp3]$	(34)
$d[ONOO^-]/dt = r_{4NO}-r_{6NO}-r_{7NO}-r_{8NO}-r_{9NO}-r_{18NO}$	(35)
$d[PTPC]/dt = -r_{19NO}$	(36)
$d[N_2O_3]/dt = -r_{11NO}+r_{12bNO}^+ - r_{12bNO}^- - r_{13NO} - r_{19NO}$	(37)
$d[casp8]/dt = -J_0+J_0^f+J_{casp8}-r_{19NO}-r_{20NO}$ (*)	(38)
$d[FeL_nNO]/dt = r_{16NO}-r_{17NO}-r_{20NO}-r_{21NO}-r_{22NO}$	(39)
$d[FeL_n]/dt = -r_{16NO}+r_{17NO}+r_{20NO}+r_{21NO}+r_{22NO}$	(40)
$d[casp9]/dt = J_4 - J_{4b} - J_5 - J_6 + J_6^f + J_{casp9} - r_{21NO}$ (*)	(41)
$d[casp3]/dt = J_6^f + J_{6b}^f - J_7 - J_8 + J_8^f - J_9 + J_9^f + J_{casp3} - r_{22NO}$ (*)	(42)
$d[cyt\ c]/dt = J_{14} - J_1 + J_{cytc} + k[PTPCact][cyt\ c_{mit}]$ where $k = 1\ \mu M^{-1}s^{-1}$ (*)	(43)

(*) J refers to fluxes of components, for details see ref [28]. $PTPC_{act}$ refers to the nonspecific pore at the mitochondria that releases cyt *c*. Note that $[PTPC_{act}] = [PTPC]_0 - [PTPC]$.
doi:10.1371/journal.pone.0002249.t005

Model II-Generation of NO-related oxidative and nitrosative species $ONOO^-$, N_2O_3, and FeL_nNO

We extended the network originally proposed by Hu and coworkers [22] by introducing additional reactions involving NO, as well as additional compounds such as the NO-related species FeL_nNO (L denotes ligands that do not contain heme), NO_2, and cytochrome *c* oxidase (C*c*Ox). Figure 1B illustrates the extended network of interactions. Table 1 lists the corresponding reactions (indexed as *(i)–(xx)*) and rate constants. The reactions *(xii)* and *(xiii)* break down the production of N_2O_3 from NO and O_2 into two steps that replace the corresponding reaction (with rate constant k_{12}) used in the model of Hu et al. [22]. Reactions *(xvi)–(xx)* are introduced in the present study. The identity of the products are not written when these compounds do not serve as reactants in any of the reactions listed in Table 1. Table 3 lists the rate laws for these reactions (the first 20 rows), which are used in the differential rate equations (rows 21–29) that control the time evolution of the concentration of the individual compounds. Model II contains 16 components. Eleven of them reach steady-state concentrations

Table 4. Reactions bridging between Models I to II (*)

Reaction	Rate constant	Reference	Reaction index
$ONOO^-$+PTPC→$PTPC_{act}$+products	k_{18NO}	accounts for $ONOO^-$ induced formation of non-specific pore associated with mitochondrial permeability transition [49]	*(xxi)*
N_2O_3+casp8→casp8.NO+FeL_n	k_{19NO}	[*78*]	*(xxii)*
FeL_nNO+casp8→casp8.NO+FeL_n	k_{20NO}	[*38*]	*(xxiii)*
FeL_nNO+casp9→casp9.NO+FeL_n	k_{21NO}	[*38*]	*(xxiv)*
FeL_nNO+casp3→casp3.NO+FeL_n	k_{22NO}	[*38*]	*(xxv)*

(*) The parameters used in the present study are $k_{18NO} = 1\ \mu M^{-1}s^{-1}$ (varying the value between 0.01 $\mu M^{-1}s^{-1}$ and 100 $\mu M^{-1}s^{-1}$ does not affect the results), $k_{19NO} = 10\ \mu M^{-1}s^{-1}$ [*78*], $k_{20NO} = k_{21NO} = k_{22NO} = 66\ \mu M^{-1}s^{-1}$ (the same value as k_{11NO}).
doi:10.1371/journal.pone.0002249.t004

within a short time interval (~20 minutes) after initiation of the simulations for $[GSH]_0 \leq 10^3$ μM and within four and half hours for $[GSH]_0 = 10^4$ μM, whereas five compounds (superoxide dismutase (SOD), glutathione peroxidase (GPX), CO_2, O_2, and cyt *c*) retain their equilibrium concentrations. Table 2 lists the initial and equilibrium concentrations different from zero, adopted in Model II, and the corresponding references.

Model III–Effects of NO-related reactions on apoptotic pathways

Model III combines Models I and II upon inclusion of the additional reactions presented in Table 4. See the highlighted compounds in Figure 1, which point to the species that couple the apoptotic and NO pathways. We note that $ONOO^-$ has a pro-apoptotic effect, while N_2O_3 and FeL_nNO (reactions labeled *(xxii)–(xxv)*) deactivate the caspases, thus inducing anti-apoptotic effects. The associated rate constants and references are given in Table 4. Table 5 provides the rate expressions (rows 30–34) and differential rate equations (rows 35–43) for these reactions and involved compounds, respectively.

The steady-state concentrations $[H^+]_\infty$ in reaction (v), $[H_2O]_\infty$ in reactions (x) and (xiv), $[NADPH]_\infty$ and $[H^+]_\infty$ in reaction (xv), $[Cu^+]_\infty$ in reaction (xvi) are incorporated into the corresponding rate constants.

Author Contributions

Conceived and designed the experiments: TB YV IB BE. Performed the experiments: EB. Analyzed the data: EB. Contributed reagents/materials/analysis tools: YV BE. Wrote the paper: EB.

References

1. Fadeel B, Orrenius S, Zhivotovsky B (1999) Apoptosis in human disease: A new skin for the old ceremony? Biochem Biophys Res Commun 266: 699–717.
2. Sanfilippo CM, Blaho JA (2003) The facts of death. Int Rev Immunol 22: 327–340.
3. Budihardjo I, Oliver H, Lutter M, Luo X, Wang X (1999) Biochemical pathways of caspase activation during apoptosis. Annu Rev Cell Dev Biol 15: 269–290.
4. Li P, Nijhawan D, Budihardjo I, Srinivasula SM, Ahmad M, et al. (1997) Cytochrome c and dATP-dependent formation of Apaf-1/caspase-9 complex initiates an apoptotic protease cascade. Cell 91: 479–489.
5. Nagata S (1997) Apoptosis by death factor. Cell 88: 355–365.
6. Kim PKM, Zuckerbraun BS, Otterbein LE, Vodovotz Y, Billiar TR (2004) 'Til death do us part: nitric oxide and mechanisms of hepatotoxicity. Biol Chem 365: 11–15.
7. Vodovotz Y, Kim PKM, Bagci EZ, Ermentrout GB, Chow CC, et al. (2004) Inflammatory modulation of hepatocyte apoptosis by nitric oxide: In vivo, in vitro and in silico studies. Curr Mol Med 4: 753–762.
8. Wang YN, Vodovotz Y, Kim PKM, Zamora R, Billiar TR (2002) Mechanisms of hepatoprotection by nitric oxide. Ann N Y Acad Sci 962: 415–422.
9. Bulotta S, Barsacchi R, Rotiroti D, Borgese N, Clementi E (2001) Activation of the endothelial nitric-oxide synthase by tumor necrosis factor-alpha. A novel feedback mechanism regulating cell death. J Biol Chem 276: 6529–6536.
10. Ceneviva GD, Tzeng E, Hoyt DG, Yee E, Gallagher A, et al. (1998) Nitric oxide inhibits lipopolysaccharide-induced apoptosis in pulmonary artery endothelial cells. Am J Physiol 275: L717–L728.
11. Dimmeler S, Rippmann V, Weiland U, Haendeler J, Zeiher AM (1997) Angiotensin II induces apoptosis of human endothelial cells. Protective effect of nitric oxide. Circ Res 81: 970–976.
12. Dimmeler S, Haendeler J, Nehls M, Zeiher AM (1997) Suppression of apoptosis by nitric oxide via inhibition of interleukin- 1beta-converting enzyme (ICE)-like and cysteine protease protein (CPP)- 32-like proteases. J Exp Med 185: 601–607.
13. Tzeng E, Kim YM, Pitt BR, Lizonova A, Kovesdi I, et al. (1997) Adenoviral transfer of the inducible nitric oxide synthase gene blocks endothelial cell apoptosis. Surgery 122: 255–263.
14. Weller R, Schwentker A, Billiar TR, Vodovotz Y (2003) Autologous nitric oxide protects mouse and human keratinocytes from ultraviolet B radiation-induced apoptosis. Am J Physiol 284: C1140–C1148.
15. Albina JE, Cui S, Mateo RB, Reichner JS (1993) Nitric oxide-mediated apoptosis in murine peritoneal macrophages. J Immunol 150: 5080–5085.
16. Messmer UK, Brune B (1996) Nitric oxide-induced apoptosis: p53-dependent and p53-independent signalling pathways. Biochem J 319 (Pt 1): 299–305.
17. Meβmer UK, Lapetina EG, Brüne B (1995) Nitric oxide-induced apoptosis in RAW 264.7 macrophages is antagonized by protein kinase C- and protein kinase A-activating compounds. Mol Pharmacol 47: 757–765.
18. Sarih M, Souvannavong V, Adam A (1993) Nitric oxide synthase induces macrophage death by apoptosis. Biochem Biophys Res Commun 191: 503–508.
19. Li JR, Billiar TR, Talanian RV, Kim YM (1997) Nitric oxide reversibly inhibits seven members of the caspase family via S-nitrosylation. Biochem Biophys Res Commun 240: 419–424.
20. Wink DA, Feelisch M, Vodovotz Y, Fukuto J, Grisham MB (1999) The Chemical Biology of Nitric Oxide. In: Colton CA, Gilbert DL, eds. Reactive Oxygen Species in Biological Systems: An Interdisciplinary approach. New York: Kluwer Academic/Plenum Publishing. pp 245–291.
21. Kim YM, Chung HT, Simmons RL, Billiar TR (2000) Cellular non-heme iron content is a determinant of nitric oxide-mediated apoptosis, necrosis, and caspase inhibition. J Biol Chem 275: 10954–10961.
22. Hu TM, Hayton WL, Mallery SR (2006) Kinetic modeling of nitric-oxide-associated reaction network. Pharm Res 23: 1702–1711.
23. Lancaster JR (1994) Simulation of the diffusion and reaction of endogenously produced nitric-oxide. Proc Natl Acad Sci U S A 91: 8137–8141.
24. Lancaster JR (1997) A tutorial on the diffusibility and reactivity of free nitric oxide. Nitric Oxide-Biology and Chemistry 1: 18–30.
25. Zhang W, Edwards A (2006) A model of nitric oxide tubulo-vascular cross-talk in a renal outer medullary cross-section. Am J Physiol Renal Physiol in press.
26. Buerk DG (2001) Can we model nitric oxide biotransport? A survey of mathematical models for a simple diatomic molecule with surprisingly complex biological activities. Annu Rev Biomed Eng 3: 109–143.
27. Aldridge BB, Haller G, Sorger PK, Lauffenburger DA (2006) Direct Lyapunov exponent analysis enables parametric study of transient signalling governing cell behaviour. Syst Biol (Stevenage) 153: 425–432.
28. Bagci EZ, Vodovotz Y, Billiar TR, Ermentrout GB, Bahar I (2006) Bistability in apoptosis: Roles of Bax, Bcl-2, and Mitochondrial Permeability Transition Pores. Biophys J 90: 1546–1559.
29. Bentele M, Lavrik I, Ulrich M, Stosser S, Heermann DW, et al. (2004) Mathematical modeling reveals threshold mechanism in CD95-induced apoptosis. J Cell Biol 166: 839–851.
30. Eissing T, Conzelmann H, Gilles ED, Allgower F, Bullinger E, et al. (2004) Bistability analyses of a caspase activation model for receptor-induced apoptosis. J Biol Chem 279: 36892–36897.
31. Fussenegger M, Bailey JE, Varner J (2000) A mathematical model of caspase function in apoptosis. Nature Biotechnol 18: 768–774.
32. Legewie S, Bluthgen N, Herzel H (2006) Mathematical modeling identifies inhibitors of apoptosis as mediators of positive feedback and bistability. PLoS Comp Biol 2: 1061–1073.
33. Rehm M, Huber HJ, Dussmann H, Prehn JHM (2006) Systems analysis of effector caspase activation and its control by X-linked inhibitor of apoptosis protein. EMBO J 25: 4338–4349.
34. Siehs C, Oberbauer R, Mayer G, Lukas A, Mayer B (2002) Discrete simulation of regulatory homo- and heterodimerization in the apoptosis effector phase. Bioinformatics 18: 67–76.
35. Stucki JW, Simon HU (2005) Mathematical modeling of caspase-3 activation and degradation. J Theor Biol 234: 123–131.
36. Rehm M, Dussmann H, Janicke RU, Tavare JM, Kogel D, et al. (2002) Single-cell fluorescence resonance energy transfer analysis demonstrates that caspase activation during apoptosis is a rapid process-Role of caspase-3. J Biol Chem 277: 24506–24514.
37. Tyas L, Brophy VA, Pope A, Rivett AJ, Tavare JM (2000) Rapid caspase-3 activation during apoptosis revealed using fluorescence-resonance energy transfer . EMBO Rep 1: 266–270.
38. Kim PKM, Zamora R, Petrosko P, Billiar TR (2001) The regulatory role of nitric oxide in apoptosis. Int Immunopharmacol 1: 1421–1441.
39. Kim YM, Talanian RV, Billiar TR (1997) Nitric oxide inhibits apoptosis by preventing increases in caspase-3-like activity via two distinct mechanisms. J Biol Chem 272: 31138–31148.
40. Mannick JB, Hausladen A, Liu LM, Hess DT, Zeng M, et al. (1999) Fas-induced caspase denitrosylation. Science 284: 651–654.
41. Rossig L, Fichtlscherer B, Breitschopf K, Haendeler J, Zeiher AM, et al. (1999) Nitric oxide inhibits caspase-3 by S-nitrosation in vivo. J Biol Chem 274: 6823–6826.
42. Stamler JS (1994) Redox signaling–nitrosylation and related target interactions of nitric-oxide. Cell 78: 931–936.
43. Benhar M, Stamler JS (2005) A central role for S-nitrosylation in apoptosis. Nat Cell Biol 7: 645–646.
44. Ghafourifar P, Asbury ML, Joshi SS, Kincaid ED (2005) Determination of mitochondrial nitric oxide synthase activity. Methods Enzymol 396: 424–444.

45. Radi R, Cassina A, Hodara R (2002) Nitric oxide and peroxynitrite interactions with mitochondria. Biol Chem 383: 401–409.
46. Nakagawa T, Shimizu S, Watanabe T, Yamaguchi O, Otsu K, et al. (2005) Cyclophilin D-dependent mitochondrial permeability transition regulates some necrotic but not apoptotic cell death. Nature 434: 652–658.
47. Newmeyer DD, Ferguson-Miller S (2003) Mitochondria: Releasing power for life and unleashing the machineries of death. Cell 112: 481–490.
48. Vieira HLA, Haouzi D, El Hamel C, Jacotot E, Belzacq AS, et al. (2000) Permeabilization of the mitochondrial inner membrane during apoptosis: impact of the adenine nucleotide translocator. Cell Death Differ 7: 1146–1154.
49. Vieira HLA, Belzacq AS, Haouzi D, Bernassola F, Cohen I, et al. (2001) The adenine nucleotide translocator: a target of nitric oxide, peroxynitrite, and 4-hydroxynonenal. Oncogene 20: 4305–4316.
50. Kim YM, de Vera ME, Watkins SC, Billiar TR (1997) Nitric Oxide protects cultured rat hepatocytes from Tumor Necrosis Factor-α induced apoptosis by inducing heat shock protein 70 expression. J Biol Chem 272: 1402–1411.
51. Chen T, Pearce LL, Peterson J, Stoyanovsky D, et al. (2005) Glutathione depletion renders rat hepatocytes sensitive to nitric oxide donor-mediated toxicity. Hepatology 42: 598–607.
52. Kim PKM, Vallabhaneni R, Zuckerbraun BS, McCloskey C, Vodovotz Y, Billiar TR (2005) Hypoxia renders hepatocytes susceptible to cell death by nitric oxide. Cell Mol Biol 51: 229–335.
53. Tiedge M, Lortz S, Drinkgern J, Lenzen S (1997) Relation between antioxidant enzyme gene expression and antioxidative defense status of insulin-producing cells. Diabetes 46: 1733–1742.
54. Oyadomari S, Takeda K, Takiguchi M, Gotoh T, Matsumoto M, et al. (2001) Nitric oxide-induced apoptosis in pancreatic beta cells is mediated by the endoplasmic reticulum stress pathway. PNAS 98: 10845–50.
55. Ermentrout B (2002) Simulating, analyzing, and animating dynamical systems. A guide to XPPAUT for researchers and students. Philedelphia: SIAM.
56. Huie RE, Padmaja S (1993) The reaction of NO with superoxide. Free Radic Res Commun 18: 195–199.
57. Fielden EM, Roberts PB, Bray RC, Lowe DJ, Mautner GN, et al. (1974) The mechanism of action of superdismutase from pulse radiolysis and electron paramagnetic resonance. Biochem J 139: 49–60.
58. Koppenol WH, Moreno JJ, Pryor WA, Ischiropoulos H, Beckman JS (1992) Peroxynitrite, a cloaked oxidant formed by nitric-oxide and superoxide. Chem Res Toxicol 5: 834–842.
59. Sies H, Sharov VS, Klotz LO, Briviba K (1997) Glutathione peroxidase protects against peroxynitrite-mediated oxidations-A new function for selenoproteins as peroxynitrite reductase. J Biol Chem 272: 27812–27817.
60. Denicola A, Freeman BA, Trujillo M, Radi R (1996) Peroxynitrite reaction with carbon dioxide/bicarbonate: Kinetics and influence on peroxynitrite-mediated oxidations. Arch Biochem Biophys 333: 49–58.
61. Squadrito GL, Pryor WA (1998) Oxidative chemistry of nitric oxide: The roles of superoxide, peroxynitrite, and carbon dioxide. Free Radic Biol Med 25: 392–403.
62. Thomson L, Trujillo M, Telleri R, Radi R (1995) Kinetics of cytochrome *c*(2+) oxidation by peroxynitrite–Implications for superoxide measurements in nitric oxide-producing biological systems. Arch Biochem Biophys 319: 491–497.
63. Jourd'Heuil D, Mai CT, Laroux FS, Wink DA, Grisham MB (1998) The reaction of S-nitrosoglutathione with superoxide. Biochem Biophys Res Commun 244: 525–530.
64. Keshive M, Singh S, Wishnok JS, Tannenbaum SR, Deen WM (1996) Kinetics of S-nitrosation of thiols in nitric oxide solutions. Chem Res Toxicol 9: 988–993.
65. Czapski G, Goldstein S (1995) The role of the reactions of NO with superoxide and oxygen in biological systems–A kinetic approach. Free Radic Biol Med 19: 785–794.
66. Licht WR, Tannenbaum SR, Deen WM (1988) Use of ascorbic acid to inhibit nitrosation: kinetic and mass transfer coefficients for an in vitro system. Carcinogenesis 9: 365–372.
67. Antunes F, Salvador A, Marinho HS, Alves R, Pinto RE (1996) Lipid peroxidation in mitochondrial inner membranes .1. An integrative kinetic model. Free Radic Biol Med 21: 917–943.
68. Gorren ACF, Schrammel A, Schmidt K, Mayer B (1996) Decomposition of S-nitrosoglutathione in the presence of copper ions and glutathione. Arch Biochem Biophys 330: 219–228.
69. Hofseth LJ, Saito S, Hussain SP, Espey MG, Miranda KM, et al. (2003) Nitric oxide-induced cellular stress and p53 activation in chronic inflammation. Proc Natl Acad Sci U S A 100: 143–148.
70. Sarti P, Arese M, Bacchi A, Barone MC, Forte E, et al. (2003) Nitric oxide and mitochondrial complex IV. IUBMB Life 55: 605–611.
71. Pou S, Tsai P, Porasuphatana S, Halpern HJ, Chandramouli GVR, et al. (1999) Spin trapping of nitric oxide by ferro-chelates: kinetic and in vivo pharmacokinetic studies. Biochim Biophys Acta 1427: 216–226.
72. Afshar RK, Patra AK, Olmstead MM, Mascharak PK (2004) Syntheses, structures, and reactivities of {Fe-NO}(6) nitrosyls derived from polypyridinecarboxamide ligands: Photoactive NO-donors and reagents for S-nitrosylation of alkyl thiols. Inorg Chem 43: 5736–5743.
73. Jones CM, Lawrence A, Wardman P, Burkitt MJ (2002) Electron paramagnetic resonance spin trapping investigation into the kinetics of glutathione oxidation by the superoxide radical: Re-evaluation of the rate constant. Free Radic Biol Med 32: 982–990.
74. Beckman JS, Koppenol WH (1996) Nitric oxide, superoxide, and peroxynitrite: The good, the bad, and the ugly. Am J Physiol-Cell Physiol 40: C1424–C1437.
75. Radi R, Denicola A, Ferrer-Sueta G, Rubbo H (2000) The biological chemistry of peroxynitrite. In: Ignarro LJ, ed. Nitric Oxide: Biology and Pathobiology. San Diego: Academic. pp 57–82.
76. De Visscher G, Rooker S, Jorens P, Verlooy J, Borgers M, et al. (2005) Pentobarbital fails to reduce cerebral oxygen consumption early after non-hemorrhagic closed head injury in rats. J Neurotrauma 22: 793–806.
77. Pourzand C, Watkin RD, Brown JE, Tyrrell RM (1999) Ultraviolet A radiation induces immediate release of iron in human primary skin fibroblasts: The role of ferritin. Proc Natl Acad Sci U S A 96: 6751–6756.
78. Wink DA, Nims RW, Darbyshire JF, Christodoulou D, Hanbauer I, et al. (1994) Reaction-kinetics for nitrosation of cysteine and glutathione in aerobic nitric-oxide solutions at neutral pH–Insights into the fate and physiological effects of intermediates generated in the NO/O_2^- reaction. Chem Res Toxicol 7: 519–525.